International Journal of Remote Sensing
Vol. 29, No. 7, 10 April 2008, 1945–1963

Taylor & Francis
Taylor & Francis Group

Shadow detection in colour high-resolution satellite images

V. ARÉVALO*†, J. GONZÁLEZ† and G. AMBROSIO‡
†Department of System Engineering and Automation, University of Málaga, Campus Teatinos, 29071, Málaga, Spain
‡Decasat Ingeniería S.L., Parque Tecnológico de Andalucía, Severo Ochoa 4, 29590 Campanillas, Málaga, Spain

(*Received 6 May 2006; in final form 31 March 2007*)

Image shadow segmentation has become a major issue in satellite remote sensing because of the recent commercial availability of high-resolution images. Detecting shadows is important for successfully carrying out applications such as change detection, land monitoring, object recognition, scene reconstruction, colour correction, etc. This paper presents a simple and effective procedure to segment shadow regions on high-resolution colour satellite images. The method applies a region growing process on a specific band (namely, the c_3 component of the $c_1c_2c_3$ colour space). To gain in robustness and precision, the region expansion also imposes a restriction on the saturation and intensity values of the shadow pixels, as well as on their edge gradients. The proposed method has been successfully tested on QuickBird images acquired under different lighting conditions and covering both urban and rural areas.

1. Introduction

High-resolution images provided by latest missions such as QuickBird, Ikonos, or OrbView have opened a new range of applications in the remote sensing field because of the possibility of extracting detailed information from the images. These applications include some that are becoming common in recent years, such as natural disaster monitoring (i.e. flood or tsunami (Adams *et al.* 2005); earthquake (Vu *et al.* 2004), etc.) or urban change detection (Del-Frate *et al.* 2005), and others that will be a real possibility in the coming years, such as urban scene reconstruction, cartography update, urban inventory, etc.

The improvement in spatial resolution of satellite imagery also implies that something inherent to images, such as shadows, take on special significance for different reasons (figure 1). On the one hand, they cause the partial or total loss of radiometric information in the affected areas, and consequently they make image-analysis processes like object detection and recognition, temporal change detection, 3D scene reconstruction, etc. more difficult or even fail. On the other hand, we may take advantage of the presence of shadows as a valuable cue for inferring 3D scene information based on the position and shape of the cast shadow, for example, for building detection, delineation, and height estimation (Irvin and McKeown 1989). It is clear, then, the convenience of accurately detecting shadowed areas in satellite images either to radiometrically correct them and/or to infer 3D information.

*Corresponding author. Email: varevalo@ctima.uma.es

International Journal of Remote Sensing
ISSN 0143-1161 print/ISSN 1366-5901 online © 2008 Taylor & Francis
http://www.tandf.co.uk/journals
DOI: 10.1080/01431160701395302

Shadow detection has received considerable attention within the computer vision field, though not much work has been done towards the application of these results to high-resolution satellite images recently available. This paper describes the main approaches to detect shadows in images, and analyses their suitability for being applied to colour satellite imagery. Based on this study, we propose a procedure that exploits invariant colour space as well as edge information to effectively and accurately detect shadows, in particular for QuickBird images (0.6 m per pixel). Additional information such as sun azimuth or object heights (DEM) is not considered here.

Very briefly, the proposed method deals with shadow detection through a region growing procedure which basically consists of two stages:

1. Small groups of pixels which are likely to be shadow are selected as seeds of shadow regions. They are obtained from a neighbourhood of local maxima in the c_3 component of the $c_1c_2c_3$ colour space. Each shadow area is then characterized by a Gaussian distribution of the c_3 values of the pixels within this region. The $c_1c_2c_3$ space, first proposed by Gevers and Smeulders (1999) for colour-based object recognition, is computed from the *RGB* representation through the following nonlinear transformations:

$$c_1 = \arctan\left(\frac{R}{\max\{G, B\}}\right) \tag{1}$$

$$c_2 = \arctan\left(\frac{G}{\max\{R, B\}}\right) \tag{2}$$

$$c_3 = \arctan\left(\frac{B}{\max\{R,G\}}\right). \tag{3}$$

2. From these seeds, the shape of the shadow region is recursively extended by adding adjacent pixels which are consistent with the above distribution. To delimit as precisely as possible the shape of the shadowed area, this process takes into account region boundary information provided by an edge detector.

One of the problems when using the c_3 component is its instability for certain colour values that leads to the misclassification of non-shadow pixels as shadow (false positives). As reported in Gevers and Smeulders (1999) and Salvador *et al.* (2004), this occurs both for pixels with low values of saturation and for pixels with extreme intensity values (either low or high). During the above two stages, to overcome this problem some components of the *HSV* space are checked. The overall approach has been successfully tested with QuickBird images acquired under different lighting conditions taken in diverse seasons, with different sun elevation angles and covering both urban and rural areas.

The remainder of this paper is organized as follows. In §2, we review some of the most representative methods of detecting shadows in digital images. In §3, we describe some colour spaces of special interest for shadow detection. In §4, the proposed method is described. In §5, we present experimental results. Finally, some conclusions and future work are outlined.

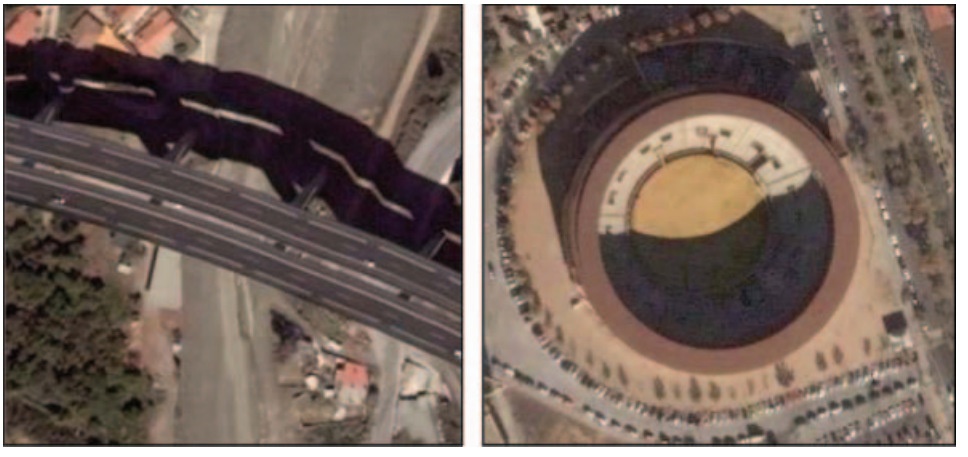

Figure 1. Shadows in high-resolution QuickBird imagery (typical urban scenes).

2. An overview of shadow detection methods

In this section, we first give a brief introduction to the nature of shadows (types and structure) and then review some previous approaches to detect shadows in digital images.

Shadow segmentation has been investigated within several computer vision applications. The first reported methods appear in the field of aerial image interpretation (Huertas and Nevatia 1988, Irvin and McKeown 1989, Wang *et al.* 1991, Koller, *et al.* 1993). With the spread of digital images in the last decade, a tremendous interest in shadow detection has emerged in applications of video stream processing, such as video surveillance, traffic control, pedestrian monitoring, etc. (Rosin and Ellis 1995, Hsieh *et al.* 2003, Prati *et al.* 2003, Salvador *et al.* 2004).

Shadows occur when objects totally or partially occlude direct light from a source of illumination. Shadows can be divided into two classes: *cast* and *self* (figure 2(*a*)). A cast shadow is projected by the object in the direction of the light source; a self shadow is the part of the object which is not illuminated by direct light. The part of a cast shadow where direct light is completely blocked by an object is called the *umbra*, while the part where direct light is partially blocked is called the *penumbra*. See Funka-Lea and Bajscy (1995) for a deeper analysis of the physics of shadows.

When dealing with aerial or satellite images, neither self-shadows nor the distinction between umbra and penumbra are of significance (figure 2(*b*)). Thus,

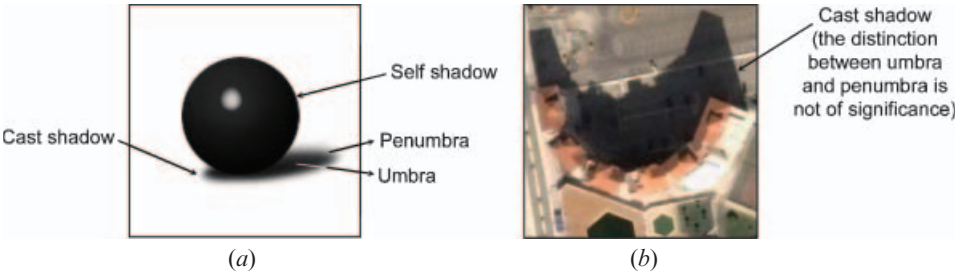

Figure 2. Different types of shadows: (*a*) indoor image and (*b*) satellite image.

most of the proposed methods presented in the remote sensing field only deal with cast shadows, and follow two general approaches, image-based methods or model-based methods (based on shadow properties), which are reviewed next.

2.1 *Image-based methods*

This approach makes use of certain image shadow properties such as colour (or intensity), shadow structure (umbra and penumbra hypotheses), boundaries, etc., without any assumption about the scene structure. Some common ways of exploiting image shadow characteristics are:

- The value of shadow pixels must be low in all the *RGB* bands. Shadows are, in general, darker than their surrounding (shadow darkness hypothesis), so they have to be delimited by noticeable borders (i.e. the shadow boundaries). Luminance information is exploited in early techniques by analysing edges (Scanlan *et al.* 1990) or histogram information (Nagao *et al.* 1979). In later works such as Salvador *et al.* (2004), these hypotheses are considered (among other information) to extract candidate shadow points in colour still images and video streaming.
- Shadows do not change the surface texture. Surface markings tend to continue across a shadow boundary under general viewing conditions. This knowledge is exploited to detect background regions which are covered or uncovered by a moving cast shadow in (Stauder *et al.* 1999).
- In some colour components (or combination of them), no change is observed whether the region is shadowed or not, that is, they are invariant to shadows. Salvador *et al.* (2004) and Sarabandi *et al.* (2004) take advantage of this feature to extract shadow boundary information (see §3 for further information about these colour representations). Another approach is presented in Huang *et al.* (2004), where the authors analyse the relationship between *RGB* bands to detect cast shadows in aerial images. Finally, in Barnard and Finlayson (2000), a new space obtained from the linear combination (ratios) of the *RGB* bands is proposed to detect shadows in indoor scenes.

2.2 *Model-based methods*

In this approach, simple shadow properties are used jointly with some a priori knowledge of the scene to derive the geometry of buildings (Irvin and McKeown 1989), vehicles (Koller *et al.* 1993, Hinz and Baumgartner 2001), pedestrians (Hsieh *et al.* 2003), etc. In a different context, there are studies that exploit cloud shadows to detect clouds (Wang *et al.* 1991, Simpson *et al.* 2000). These methods make assumptions about the observed scenes and, sometimes, about some image acquisition parameters such as camera orientation, date and daytime of acquisition, etc. Examples of how to apply such knowledge are:

- One or more edges of the cast shadow are oriented exactly in the light direction. In Jiang and Ward (1994) and Massalabi *et al.* (2004), both intensity and geometry constraints are used to detect and classify shadows in images of constrained, simple environments.
- Shadow size depends on the light source direction and the object's height. In Stevens *et al.* (1995), the authors present a technique which takes into account such information in combination with imprecise terrain maps to determine the

probability that a given point in an aerial photographs is either in sunlight or in shadow.

In general, the shadow detection techniques proposed in these works are quite simplified processes (typically, thresholding) which are usually part of a more complex system that refines the shadow area (along with the model of the object that has cast it) through a hypothesis-verification framework. In some works, the accuracy in confining the shadow region is not important, since it is only employed as a cue for the presence of buildings (typically, detecting shadows is easier than detecting buildings, pedestrians, cars, etc.).The main limitation of these methods is that they are designed for specific applications and for a particular type of object. Therefore, in complex scenes, as is usually the case for high-resolution images, they are not general enough for coping with the great diversity of geometric structures they may contain.

Our technique for shadow detection is a pure image-based method, since we exclusively apply image properties. In particular, we exploit both a shadow invariant colour component and edge information. Although the Sun azimuth and sensor/camera localization are typically available for satellite images (i.e. in QuickBird), we do not make use of this information since, in general, it is not possible to derive precise model of the acquired area (in most cases, the 3D geometry of scene is unknown or of a great complexity).

Next, we analyse the c_3 component of the $c_1c_2c_3$ colour space and its suitability for being applied to shadow detection in colour high-resolution satellite images.

3. c_3 colour component

Colour can be represented in a variety of three dimensional spaces, such as *RGB*, *HSV*, *XYZ*, $c_1c_2c_3$, $l_1l_2l_3$, *YCrCb*, *Lab*, *Luv*, etc. (Ford and Roberts 1998). Each colour space is characterized by interesting properties which make it especially appropriate for a specific application. Among these properties, we can highlight the invariant features. For example, some colour spaces are invariant to changes in the imaging conditions including viewing direction, object surface orientation, lighting conditions, and shadows. Traditional colour spaces such as normalized-*RGB* (*rgb*), hue and saturation (from *HSV*), and, more recently, $c_1c_2c_3$ (Gevers and Smeulders 1999) are colour representations that have revealed some kind of shadow invariant property. Of remarkable effectiveness is the latter, $c_1c_2c_3$, which has been successfully used by Salvador *et al.* (2004) to extract shadows in simple images with few single-colour objects and a flat (non-textured) background. Obviously, these premises cannot be assumed in high-resolution colour satellite images where the observed scenes are highly textured, objects may have many different colours, and the scene, in general, is very complex (figure 3). In Sarabandi *et al.* (2004), the authors also employ this representation to extract shadow boundaries in high-resolution images by means of a texture filter.

To evaluate the limitations of the $c_1c_2c_3$ space for shadow detection, we have performed tests over a broad set of QuickBird images, acquired under different lighting conditions and covering both urban and rural areas. The results of our tests verifies the suitability of the c_3 component to identify shadowed regions which produce a much higher response than those non-shadowed (figure 3). Despite these promising possibilities, our tests have also revealed the following problems:

Figure 3. Typical urban scenes that illustrate the complexity of high-resolution colour satellite images (e.g. highly textured, objects may have many different colours, etc.) and their corresponding c_3 components. Local maxima produced by saturated white areas (bottom left) and swimming pools (bottom right) are marked in both images.

- The c_3 band is quite noisy, which causes the misclassification of shadow pixels as non-shadow (true negatives) as well as inaccuracies in the shadow boundaries.
- Equation (3) becomes unstable for low saturation (S) values (i.e. grey levels), which causes the misclassification of non-shadow pixels as shadow (false positives) (e.g. asphalt, concrete areas, etc.). This behaviour has also been reported by Gevers and Smeulders (1999).
- Colours close to blue (high values of B) are wrongly detected as shadows (false positives). In our test images, typically this occurs for blue water (i.e. swimming pools), as illustrated in figure 3.

To overcome the above problems, in our approach we incorporate the following two actuations:

- To minimize the noise effect, the c_3 image is smoothed, and we make use of the intensity image gradient to define more precisely the shadow areas.
- We check the components S and V (from HSV) and do not classify a pixel as shadow if it is one of the above cases. This may give rise to small gaps in a shadow region, but it is a minor cost to pay for avoiding false positives, especially since these small gaps may be filled later by a morphological filter.

Next, we describe the developed method, which is based on the segmentation of a smoothed c_3 image while taking into account the aforementioned considerations.

4. Description of the proposed method

Figure 4 shows the block diagram of the proposed system which comprises the three stages described next. The system has been successfully implemented in C++ and makes use of *The OpenCV Library* (Open Source Computer Vision Library; visit http://www.sourceforge.net/projects/opencvlibrary for further information) to deal with the image-processing operations.

4.1 *Pre-processing stage*

The system input is an RGB image from which the following components are computed: c_3, saturation (S) and intensity (V). The c_3 image is convolved with a 3×3 average kernel to minimize the effects of noise (figure 5(c)), and the magnitude of gradient of the intensity image (V) is computed by a 3×3 Sobel detector (figure 5(d)).

4.2 *Shadow detection stage*

For segmenting the shadows, we apply a region growing process over the smoothed c_3 component. A generic region growing process starts with a small group of pixels (called seed-window) and recursively adds neighbour pixels as long as they confirm certain region membership rules. This technique is particularly suitable for our problem because many shadow regions may exist throughout the image, and each may have different radiometric profiles (shadow strength may vary from one zone of the image to another). Obviously, one of the pivotal points when applying this

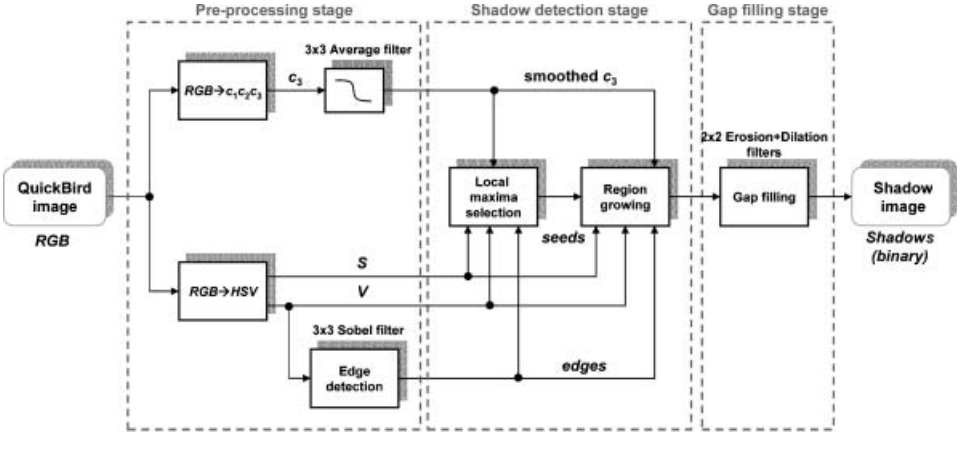

Figure 4. Structure of the proposed shadow detection system.

technique is that of reliably placing the seeds in the image: at least one per shadow region (irrespective if they are redundant) and no seed at non-shadow pixels. Next, we describe our implementation of this technique in more depth.

4.2.1 Seed selection. In our implementation, a seed is a square region (window) of 5×5 pixels. It is placed at pixels of the smoothed c_3 image that confirm the following conditions:

1. The centre is a local maximum, and its 5×5 neighbourhood must have values higher than the mean of the whole c_3 image. The size of this window gives the minimum size allowed for the shadows, for example, $3 \times 3\,\mathrm{m}^2$ for a QuickBird image of 0.6 m per pixel of resolution.
2. The mean of the intensity (V) component of the window's pixels must be lower than a certain threshold T_V (hypothesis of *shadow darkness*). In the same way, the mean of the saturation (S) component must be higher than a threshold T_S, to avoid the instability of c_3 (equation (3)) for low-saturation colours.
3. None of the window's pixels must belong to another previous seed-window.

These values have been empirically set to $T_V=0.35$ and $T_S=0.02$ within the range [0,1]. In §5, we analyse how much the variation of these thresholds affects the shadows obtained.

Each of the seed-windows is now taken as a shadow prototype which is characterized by a Gaussian distribution $N(\hat{c}_3,\sigma)$ estimated from their c_3 values (figure 6). The process described below relies on this information for growing the seeds through the shadow region.

The above conditions make it highly likely that the seed-window corresponds to a shadow. Since, in a typical shadow region, several seeds are usually identified, we do not mind very much if some of them are ruled out by these demanding premises: the important point is not to generate false positive seeds. When several seeds are placed within the same shadow, they eventually meet each other during the growing process and end up being a single region.

4.2.2 Region growing. This procedure is recursively executed for all the eight neighbours of the boundary pixels of a growing region. Starting with the seed-window, a pixel is classified as shadow and added to the region if it satisfies the following conditions:

1. It has not previously added to any shadow region already grown.
2. It is below a certain Mahalanobis distance d_0 from the mean $\hat{c}_3$ of the region, that is:

$$\frac{|c_3-\hat{c}_3|}{\sigma} < d_0. \tag{4}$$

   Notice that higher values of σ indicate a higher dispersion of c_3 within the region, and thus we tolerate larger deviation from the mean $\hat{c}_3$. A value of $d_0=3$ has shown to produce good results.
3. The magnitude of the gradient of V is below a given threshold $T_E=0.30$, that is, it is not a shadow boundary pixel. (We have also tried with the gradient of the c_3 smoothed image but because of the noise—still there, in spite of the smoothing—the results are not reliable enough.)
4. It satisfies the conditions imposed to the seed pixels regarding the values of S and V (see §4.2.1).

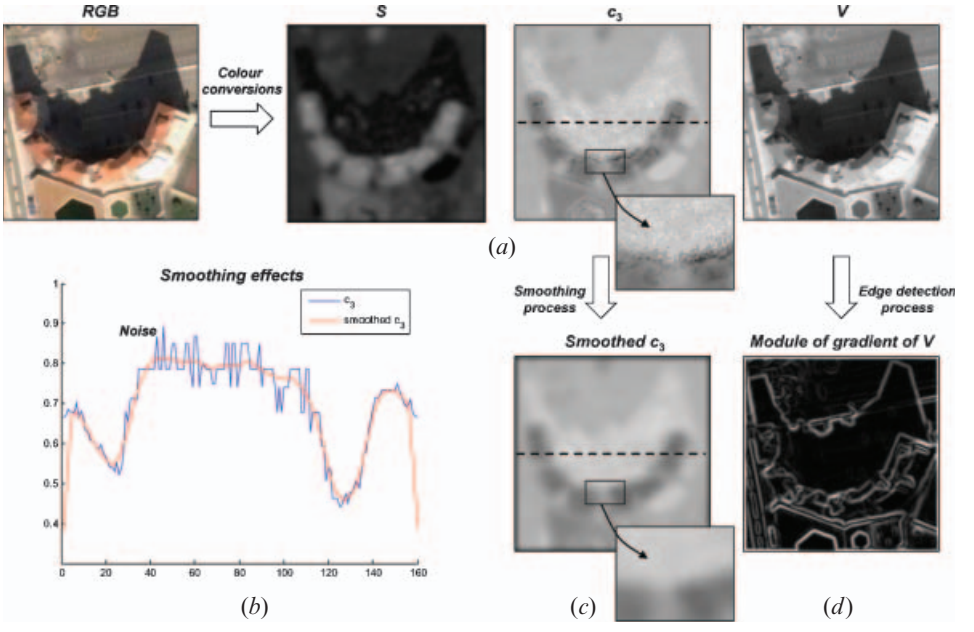

Figure 5. (*a*) Colour components computed from the *RGB* image. (*b*) Horizontal scan lines which illustrate the effects of smoothing stage in the c_3 component. The images (*c*) and (*d*) show the results of the image processes described in section 3, that is, the smoothed c_3 component and the module of gradient of V, respectively.

If the pixel is incorporated into the region, the Gaussian distribution $N(\hat{c}_3,\sigma)$ is updated with its c_3 value. The process ends when none of the neighbour pixels has been added to the region.

Notice that, during the growing process of a particular seed, pixels of different seed-windows not processed yet can be evaluated as any other image pixel. If their inclusion in the region is accepted, that seed is removed from the list of remaining seeds to be grown. We have checked that there is not much difference in the results between this sequential implementation and a concurrent one since, in the end, all of the obtained regions are going to be merged into a single indistinctive one after the gap filling stage (to be described next).

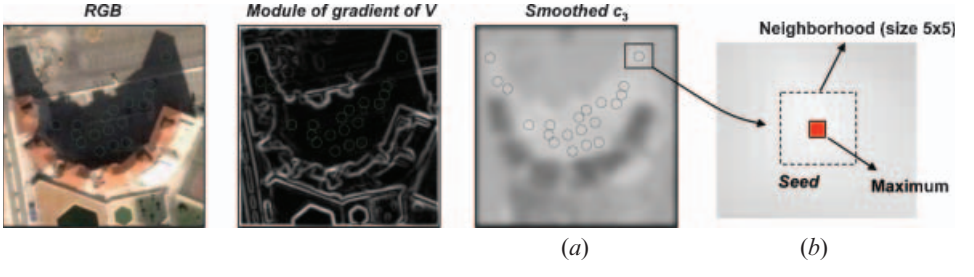

Figure 6. (*a*) Shadow seeds identified in the smoothed c_3 component. (*b*) A shadow seed window.

Figure 7 illustrates the growing process in one dimension. It displays several scan lines: the components c_3, S, and V, respectively, and the module of gradient of the V image. We can observe three detected seed-windows and the shadow boundaries (indicated by vertical lines) where the region growing process ends because of some of the above-mentioned conditions are not met.

Figure 8(*a*) shows the evolution of a Gaussian distribution during the growing of a shadow region. As we can observe, the distribution parameters $\hat{c}_3$ and σ update their values when new shadow pixels are added to the initial seed. This procedure allows us to dynamically characterize the shadow area and to control the growing process efficiently, in spite of the noisy nature of the c_3 component. Figure 8(*b*) shows two adjacent shadow regions generated after growing two seeds placed in different textured areas within the same cast shadow.

4.3 *Gap-filling stage*

After the region growing, small gaps in the shadow region may appear because of the misclassification of shadow pixels (true negatives) (figure 9(*b*)). To correct this, we apply sequentially a typical pair of morphological operations over the binary shadow image consisting of a dilatation with a 2×2 filter, followed by a 2×2 erosion filter (Sonka *et al.* 1998). This fills in gaps up to 2 pixels wide while preserving the original boundaries (as illustrated in figure 9(*c*)).

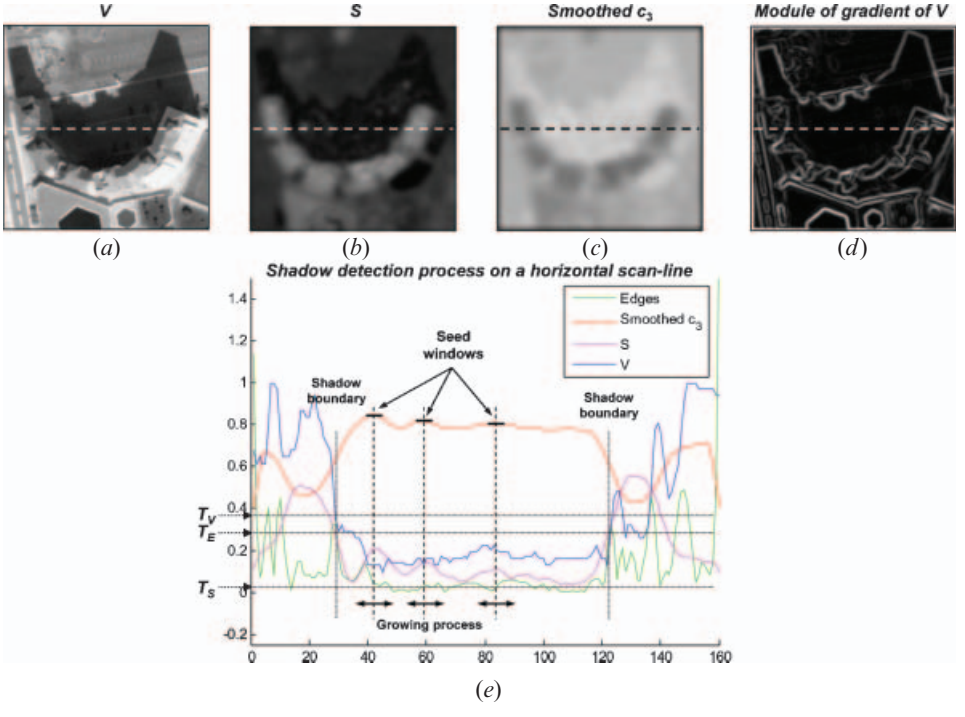

Figure 7. Seed selection and growing processes are illustrated on a horizontal scan-line of the image: (*a*) the V component, (*b*) the S component, (*c*) the smoothed c_3 component and (*d*) the module of gradient of V. (*e*) All scan-lines plotted together and the limits according to the termination conditions.

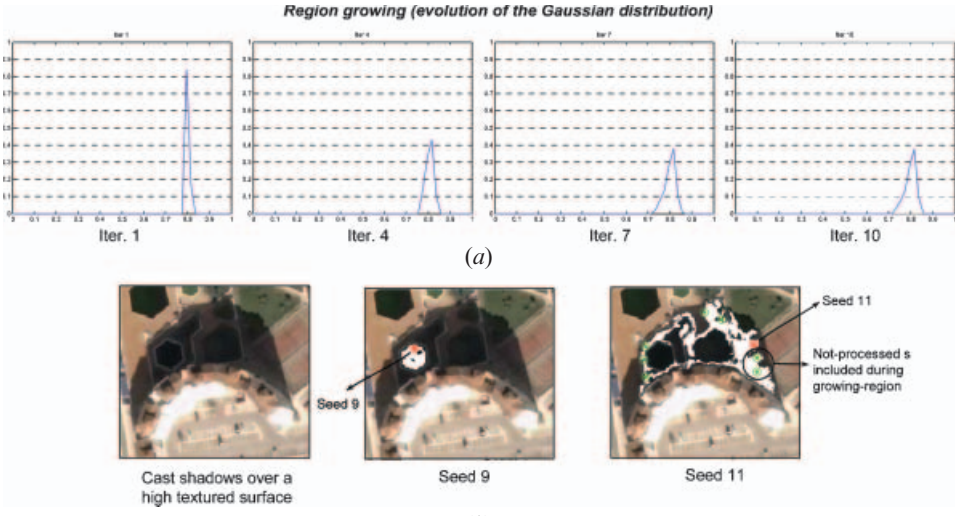

Figure 8. (*a*) Evolution of the Gaussian distribution $N(\hat{c}_3,\sigma)$ during the growing process of a shadow region (10 iterations). (*b*) Shadow regions generated after growing two seeds identified in a cast shadow. Observe that when growing seed 11 (the right-most image), other seeds not processed yet are included in the region and, consequently, discarded as seeds for further growing.

5. Experimental results

The proposed method has been tested with a variety of QuickBird pan-sharpen colour images acquired under different lighting conditions (diverse seasons and sun elevation angles) and covering both urban and rural areas. To quantify the effectiveness of the method, we have chosen one of 1024×1024 pixels, of a typical urban scene where significant shadow regions appear. The image also contains low saturation areas (concrete, asphalt, etc.), saturated white areas, and dark non-shadow regions that may confuse the shadow detection method. A 'ground data' *shadow image* is obtained by manually selecting the shadowed areas with the

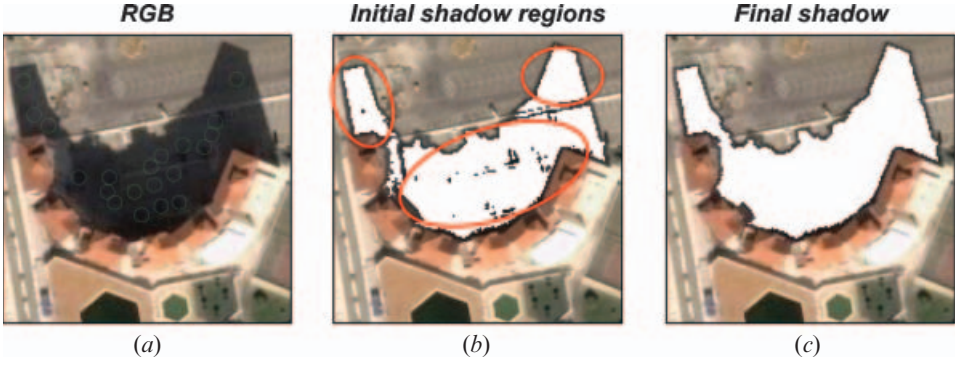

Figure 9. (*a*) Shadow seeds identified in the smoothed c_3 component during the seed selection stage (plotted on the *RGB* image). (*b*) Shadow regions generated by the growing region stage. Observe how a single shadow may appear disconnected. (*c*) Shadow region provided by the gap-filling process.

selection tools included in a well-known image-processing package (Adobe® Photoshop®). Through a pixel-by-pixel comparison with this shadow image we have classified the pixels of our test images as true/false positive/negative (TP, TN, FP, and FN). A pixel is set to be TP/FP if it is correctly/erroneously detected as shadow, and TN/FN when it is correctly/erroneously detected as non-shadow. Both true positives (TP) and true negatives (TN) are correct classifications, while the others are misclassifications.

Three statistics that capture the goodness of these four values are: the Producer's Accuracy (PA), also called *sensitivity* (Kanji 1999), the Consumer's Accuracy (CA), and the Overall Accuracy (OA), which are defined as follows:

$$\mathrm{PA} = \frac{\mathrm{TP}}{\mathrm{TP}+\mathrm{FN}} \times 100 \tag{5}$$

$$\mathrm{CA} = \frac{\mathrm{TP}}{\mathrm{TP}+\mathrm{FP}} \times 100 \tag{6}$$

$$\mathrm{OA} = \frac{\mathrm{TP}+\mathrm{TN}}{\mathrm{TP}+\mathrm{FP}+\mathrm{TN}+\mathrm{FN}} \times 100. \tag{7}$$

For completeness, we also include the *specificity* (SP) (Kanji 1999), which is defined as:

$$\mathrm{SP} = \frac{\mathrm{TN}}{\mathrm{TN}+\mathrm{FP}} \times 100. \tag{8}$$

Notice that TP + FN and TN + FP are the shadow and non-shadow ground data, respectively. Consequently, the producer's accuracy indicates the probability of the method of correctly classifying a pixel as shadow among those which are actually shadow, while the specificity gives us the probability of the method of correctly classifying a pixel as non-shadow among those which are actually non-shadow. Thus, the greater these two statistics, the better the detection process.

Since our method makes use of information from edges and different colour components, it is of interest to evaluate their contributions to the results. Table 1 shows the performance of the method for different combinations of the information

Table 1. Statistics of applying our shadow detection method with the thresholds reported in §4, to an image of size 1024 × 1024 that includes the pieces shown in figures 11 and 13.

Information used	TP	FN	FP	TN	PA	CA	OA	SP
c_3	20.46	2.17	21.60	55.77	90.41	48.64	76.23	72.08
c_3, S	20.15	2.47	16.07	61.30	89.07	55.65	81.45	79.23
c_3, edges	19.44	3.19	11.21	66.16	85.92	63.43	85.60	85.51
c_3, V	20.36	2.27	7.21	70.16	89.98	73.85	90.52	90.68
c_3, S, edges, V	18.36	4.27	1.85	75.53	81.15	90.94	93.89	97.62

TP, FN, FP, and TN are computed as percentages with respect to the total number of image pixels, while PA (Producer's Accuracy), CA (Consumer's Accuracy), and OA (Overall's Accuracy) are obtained through their definition formulas in §5. The ground data shadow pixels (TP + FN) equal 22.63%.

managed by the region growing procedure. For example, $<c_3, V>$ refers to the application of the region growing without taking into account the restrictions regarding the gradient of V (edges) and saturation. This table reveals the importance of including, apart from the c_3 component, the three additional constraints (for S, V and gradient values). Among these three constraints, it is remarkable the effect of the hypothesis of darkness of shadows (the V value below a threshold T_V), which produces an important decrease in the percentage of FP. In this implementation, the thresholds for the set of constraints (c_3, S, Edges, V) have been selected to be very restrictive in not detecting non-shadow pixels as shadow (high consumer accuracy), at the cost of missing some true shadows (producer's accuracy); observe in the last row of table 1 that the percentage of TP falls slightly.

Another issue of concern is how the threshold selection affects the performance of the method. To analyse this subject, we have conducted a set of trials that involve running the shadow detection process for a range of values of a given threshold, while the rest of them remain fixed (with the values proposed in §4.2). Figure 10

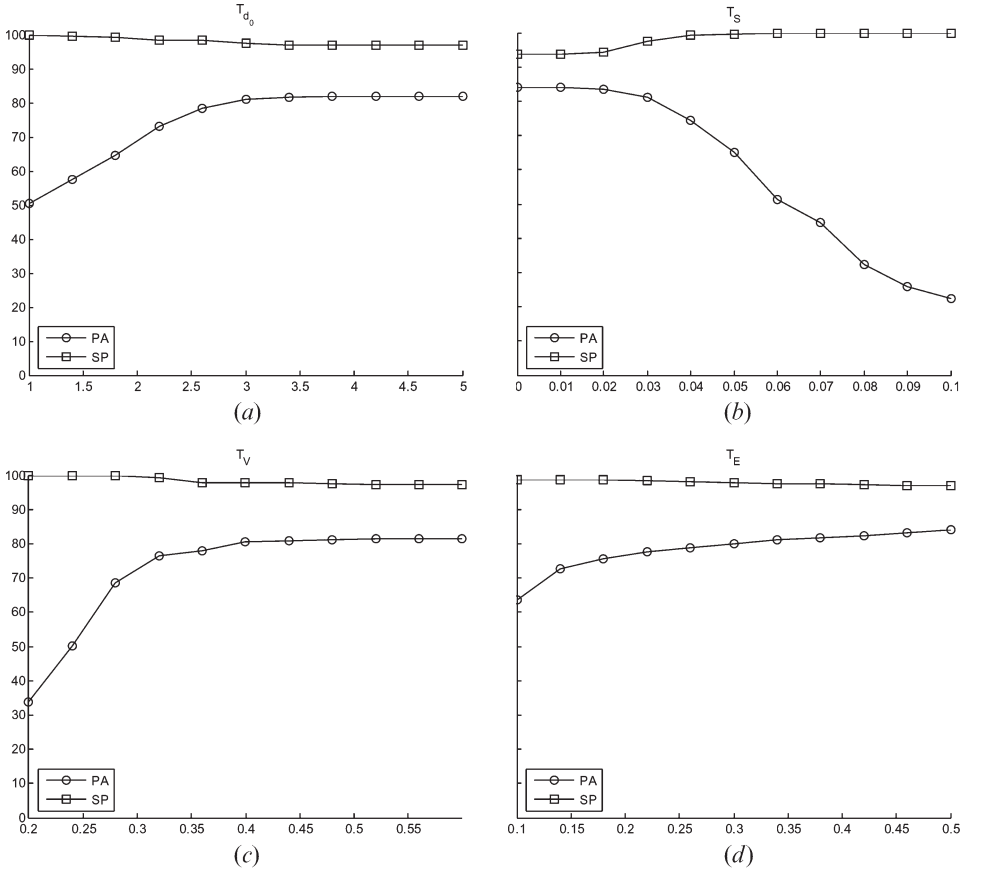

Figure 10. Producer's accuracy (PA) and specificity (SP) indices for a set of trials where the proposed shadow detection process was executed using a range of values of a given threshold, while the rest of them remain fixed (with the values proposed in section 4.2). The image is a pan-sharpened QuickBird of 1024×1024 pixels corresponding to an urban area (see the text for more details).

shows the results of these experiments in terms of the producer's accuracy and specificity indices, where the following points can be highlighted:

1. The specificity is always high regardless of the threshold value (for all the plots), because the TP remains small in comparison with the TN (its slight drop may be due to a significant increase in the FP). Notice that, when the specificity decreases, the producer's accuracy increases, so we must select the threshold to balance between these two opposite behaviours: good in detecting shadows or in not detecting non-shadows.
2. With the exception of the edge threshold (T_E), all the plots present 'flat' intervals where the threshold values can vary without affecting the PA of the output of the procedure too much. For example, any value of T_S can be selected within the range [0.01–0.03] giving almost the same result. This is important, because it allows us certain tolerance in the selection of these parameters.
3. From our tests with other different images (not shown here) we have verified that optimal threshold values may slightly change with their brightness, contrast, colour balance, etc. However, it has also been checked that intermediate thresholds in the middle of these intervals produce satisfactory (though not optimal) results for a wide variety of images.

Next, to show visual results of the proposed method, we have selected two small images of the city of Puerto de Santa María, Cádiz, Spain: one is a piece of that used in the above experiments which covers a typical urban area (i.e. high buildings, green areas, parking, etc.) that allows us to illustrate the method performance in the presence of saturations and dark regions (figure 11(*a*)); and the other is a residential area with buildings and some woods, which is particularly interesting for checking the method behaviour on high-textured areas and with small, irregular shadows (figure 12(*a*)). The following particular points of interest can be remarked from these figures:

- Figure 11(*b*) shows large shadow regions which are reasonably well delimitated. Shadows in this image are not easy to detect because they are cast over a highly textured surface (as in the bottom-left building) and also because some elements could be wrongly classified as shadows (i.e. the dark hexagons, the saturated side of the buildings, etc.).
- In Figure 12(*b*), although some small shadows have not been detected, the method performs quite acceptably given the difficulty, even for a human eye, to distinguish between tree crowns and shadows. The undetected shadows are because no seed was placed in them. This could be corrected to a certain extent with a less restrictive set of thresholds and/or a smaller seed-window, but at the expenses of producing more false positive regions and an increase in the computational time (because of the larger number of seeds). For example, if we use a 3×3 seed-window instead of a 5×5 one with the image of figure 12(*a*), the producer's accuracy improves 4%, but now some false positive small regions appear, and the computational time rises from 6.75 s to 9.76 s.

Finally, we have compared the performance of our method against the techniques proposed by Huang *et al.* (2004) and Sarabandi *et al.* (2004), previously commented in §2.1 and 3. The former applies an area-based algorithm in the *RGB* space, while the latter searches for shadow boundaries in the $c_1c_2c_3$, as our method does. We have

(*a*) (*b*)

Figure 11. (*a*) QuickBird image from a high-textured urban area which contains cast shadows, intensity saturations, and dark regions. (*b*) Shadows detected by the proposed method using the set of parameter reported in section 4.2.1 (number of seeds=69, PA=83.54%, SP=99.84%, and CPU time=10.96 s).

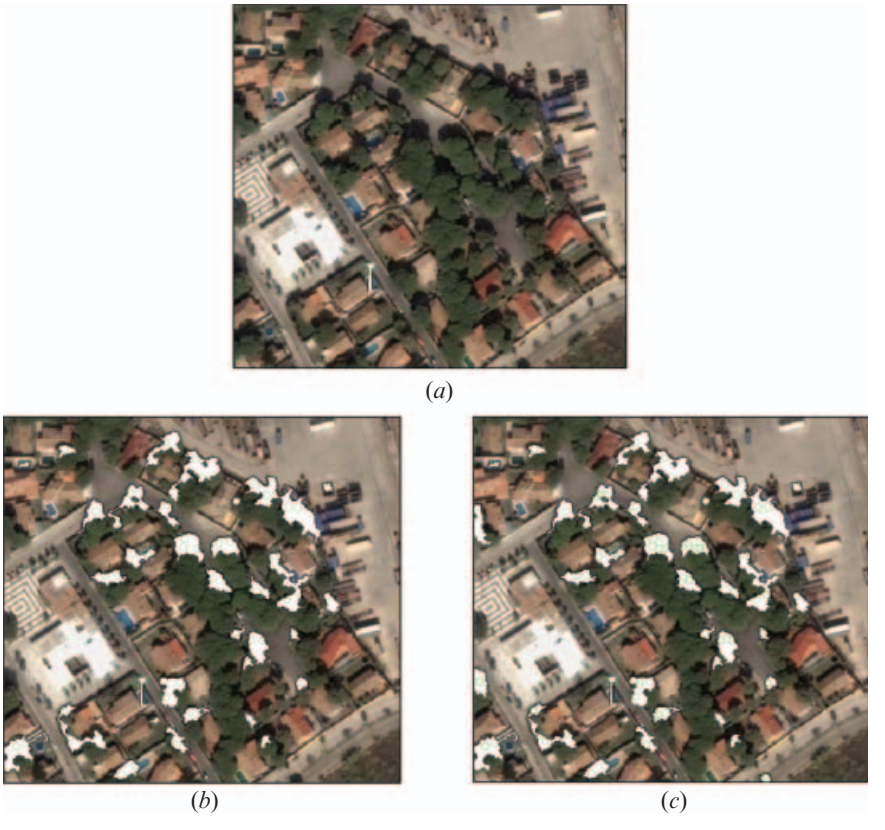

(*a*)

(*b*) (*c*)

Figure 12. (*a*) QuickBird image from a high-textured residential area which contains regular buildings and woods. (*b*) Shadows detected by the proposed method using the set of parameter reported in section 4.2.1 (number of seeds=57, PA=49.80%, SP=96.39%, and CPU time=6.75 s). (*c*) Shadows generated using a seed size of 3×3 pixels (instead of a 5×5), and the same set of parameters (number of seeds=94, PA=53.35%, SP=96.18%, and CPU time=9.76 s).

Table 2. Comparison of the performance of our method with two other recent techniques proposed in the remote sensing field.

Method	TP	FN	FP	TN	PA	CA	OA	SP
RGB-based method (Huang *et al.* 2004)	15.49	7.14	2.63	74.74	68.45	85.49	90.23	96.60
$c_1c_2c_3$-based method (Sarabandi *et al.* 2004)	17.39	5.23	5.32	72.05	76.87	76.56	89.44	93.12
Our method	18.36	4.27	1.85	75.53	81.15	90.94	93.89	97.62

Huang *et al.* (2004) worked on the *RGB* colour space, and Sarabandi *et al.* (2004) used (as we do) the $c_1c_2c_3$ representation. The test image is the same as that in table 1.

chosen these two because they are recent, work with high-resolution aerial and satellite imagery, and describe the algorithms with enough detail for them to be implemented. Table 2 summarizes the results of this comparison in terms of their accuracies. Two major points can be highlighted: (a) the advantage of employing the $c_1c_2c_3$ space instead of the *RGB* one, which presents the lowest statistics (PA, CA, OA, SP), and (b) the good performance of our proposal, which excels the other two. Figure 13 shows the resulting shadows of these two methods, where it is noticeable the misclassification they produce for pixels belonging to swimming pools and low-saturation areas (e.g. terrace roofs).

6. Conclusions and future work

In this paper, we have presented a procedure for automatically detecting shadows in high-resolution satellite images, in particular for QuickBird. The proposed approach is based on other works, reported in the computer vision literature, that were developed for quite different images. We have exploited the response of one of the components (c_3) of a colour space named $c_1c_2c_3$ to shadowed pixels. To overcome the limitations that the c_3 band presents, a region-growing procedure has been developed that also takes into account some components of other colour space (S and V).

Although our approach needs the manual selection of certain parameters (thresholds), they do not need to be tuned very precisely to achieve satisfactory results. Experimentally, we have verified the reliability and effectiveness of the method for a wide variety of image conditions, though the rate of true negatives (non-detected true shadows) is still high for some applications like urban change detection.

In future research, we would like also to exploit shadow areas for both restoring the radiometric information and for inferring 3D information from them (e.g. the height of the buildings).

Acknowledgements

The authors would like to thank the reviewers whose comments have significantly improved this manuscript. The ©DigitalGlobe QuickBird imagery used in this

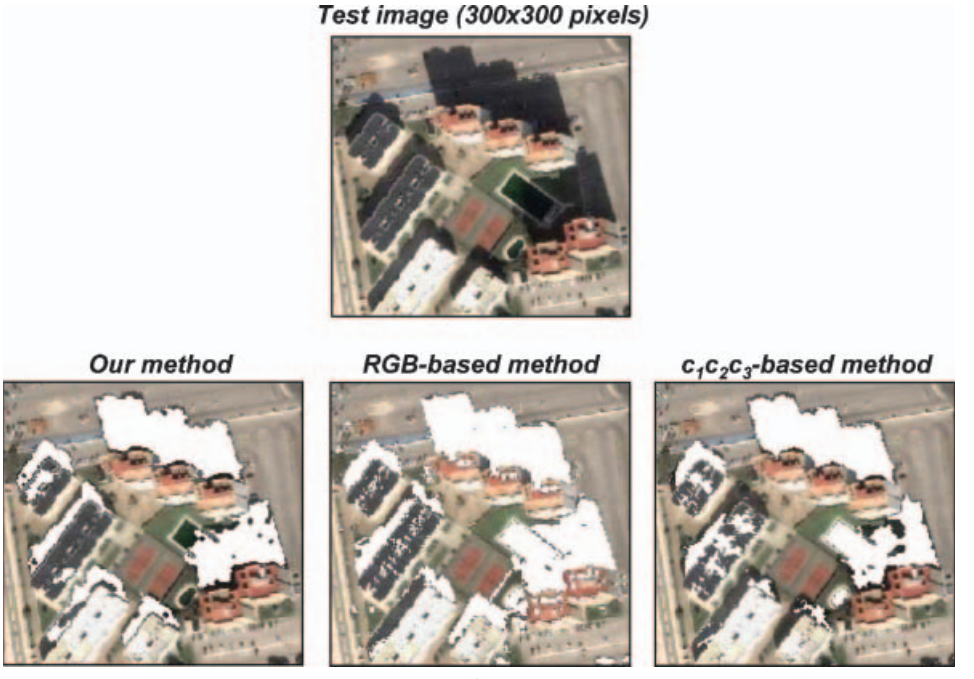

Figure 13. Comparison of the shadow areas detected by our algorithm (in (*a*)) and two other methods: (*b*) using the *RGB* space (Huang *et al.*, 2004) and (*c*) using the $c_1c_2c_3$ space (Sarabandi *et al.*, 2004). Observe the wrong classification in (*b*) and (*c*) of the swimming pools as well as some low-saturated areas in the terrace roofs.

study is distributed by Eurimage, SpA (www.eurimage.com) and provided by Decasat Ingenieria S.L., Málaga, Spain (www.decasat.com).

References

ADAMS, B.J., WABNITZ, C., GHOSH, S., ALDER, J., CHUENPAGDEE, R., CHANG, S.E., BERKE, P.R. and REES, W.E., 2005, Application of Landsat 5 and high-resolution optical satellite imagery to investigate urban tsunami damage. In *III International Workshop on Remote Sensing for Post-Disaster Response*, 12–13 September, Chiba, Japan.

BARNARD, K. and FINLAYSON, G., 2000, Shadow identification using color ratios. In *IS&T/SID VIII Color Imaging Conference: Color Science, Systems and Applications*, pp. 97–101.

DEL-FRATE, F., SCHIAVON, G. and SOLIMINI, C., 2005, Change detection in urban areas with QuickBird imagery and neural networks algorithms. In *III ISPRS International Symposium Remote Sensing and Data Fusion Over Urban Areas (URBAN'05)*, 14–16 March, Tempe, AZ.

FORD, A. and ROBERTS, A., 1998, Colour space conversions. *Technical report*, Westminster University, London.

FUNKA-LEA, G. and BAJSCY, R., 1995, Combining colour and geometry for the active, visual recognition of shadows. In *V IEEE International Conference on Computer Vision (ICCV'95)*, 20–23 June, Boston, MA, pp. 203–209.

GEVERS, T. and SMEULDERS, A.W.M., 1999, Colour-based object recognition. *Pattern Recognition*, **32**, pp. 453–464.

HINZ, S. and BAUMGARTNER, A., 2001, Vehicle detection in aerial images using generic features, grouping, and context. In *Pattern Recognition 2001 (DAGM Symposium 2001)*, **2191** of *Lecture Notes in Computer Science* (Berlin: Springer), pp. 45–52.

HSIEH, J., HU, W., CHANG, C. and CHEN, Y., 2003, Shadow elimination for effective moving object detection by gaussian shadow modeling. *Journal of Image and Vision Computing*, **21**, pp. 505–516.

HUANG, J., XIE, W. and TANG, L., 2004, Detection of and compensation for shadows in coloured urban aerial images. In *V IEEE World Congress on Intelligent Control and Automation*, 15–19 June, Hangzhou, P.R. China, pp. 3098–3100.

HUERTAS, A. and NEVATIA, R., 1988, Detecting buildings in aerial images. *Computer Vision, Graphics and Image Processing*, **41**, pp. 131–152.

IRVIN, B. and MCKEOWN, J.R., 1989, Methods for exploiting the relationship between buildings and their shadows in aerial imagery. *IEEE Transactions on System, Man and Cybernetics*, **19**, pp. 1564–1575.

JIANG, C. and WARD, M.O., 1994, Shadow segmentation and classification in a constrained environment. *CVGIP: Image Understanding*, **59**, pp. 213–225.

KANJI, G.K., 1999, *100 Statistical Tests* (Thousand Oaks, CA: SAGE).

KOLLER, D., DANIILIDIS, K. and NAGEL, H., 1993, Model-based object tracking in monocular image sequences of road traffic scenes. *International Journal of Computer Vision*, **10**, pp. 257–281.

MASSALABI, A., HE, D.C., BÉNIÉ, G.B. and BEAUDRY, É., 2004, Restitution of information under shadow in remote sensing high space resolution images: Application to IKONOS data of Sherbrooke city. In *XX ISPRS Congress*, 12–23 July, Istanbul, Turkey.

NAGAO, M., MATSUTYAMA, T. and IKEDA, Y., 1979, Region extraction and shape analysis in aerial photographs. *Computer Vision Graphics and Image Processing*, **10**, pp. 195–223.

PRATI, A., MIKIC, I., TRIVEDI, M.M. and CUCCHIARA, R., 2003, Detecting moving shadows: algorithms and evaluation. *IEEE Transactions on Pattern Analysis and Machine Intelligence*, **25**, pp. 918–923.

ROSIN, P.L. and ELLIS, T., 1995, Image difference threshold strategies and shadow detection. In *1995 British Conference on Machine Vision*, July, Birmingham, UK, **1**, pp. 347–356.

SALVADOR, E., CAVALLARO, A. and EBRAHIMI, T., 2004, Cast shadow segmentation using invariant colour features. *Computer Vision and Image Understanding*, **95**, pp. 238–259.

SARABANDI, P., YAMAZAKI, F., MATSUOKA, M. and KIREMIDJIAN, A., 2004, Shadow detection and radiometric restoration in satellite high resolution images. In *IEEE International Geoscience and Remote Sensing Symposium (IGARSS)*, 20–24 September, Anchorage, AL, **6**, pp. 3744–3747.

SCANLAN, J.M., CHABRIES, D.M. and CHRISTIANSEN, R., 1990, A shadow detection and removal algorithm for 2-D images. In *IEEE International Conference on Acoustic, Speech, and Signal Processing (ICASSP)*, 3–6 April, Albuquerque, NM, **4**, pp. 2057–2060.

SIMPSON, J.J., JIN, Z. and STITT, J.R., 2000, Cloud shadow detection under arbitrary viewing and illumination conditions. *IEEE Transactions on Geoscience and Remote Sensing*, **38**, pp. 972–976.

SONKA, M., HLAVAC, V. and BOYLE, R., 1998, *Image Processing, Analysis and Machine Vision*, 2nd ed., pp. 188–199 (London: International Thomson Computer Press).

STAUDER, J., MELCH, R. and OSTERMANN, J., 1999, Detection of moving cast shadows for object segmentation. *IEEE Transactions on Multimedia*, **1**, pp. 65–77.

STEVENS, M.R., PYEATT, L.D., HOULTON, D.J. and GOSS, M., 1995, Locating shadows in aerial photographs using imprecise elevation data. *Computer Science Technical Report CS-95–105*, Colorado State University.

VU, T.T., MATSUOKA, M. and YAMAZAK, F., 2004, Shadow analysis in assisting damage detection due to earthquakes from QuickBird imagery. In *XX ISPRS Congress*, 12–23 July, Istanbul, Turkey, pp. 607–610.

WANG, C., HUANG, L. and ROSENFELD, A., 1991, Detecting clouds and cloud shadows on aerial photographs. *Pattern Recognition Letters*, **12**, pp. 55–64.